# FRICTION FAULT DETECTION OF AN ELECTROHYDROSTATIC ACTUATOR

**S. A. Gadsden***
**Y. Song**
**K. R. McCullough**
**S. R. Habibi**
Department of Mechanical Engineering
McMaster University
Hamilton, Ontario, Canada, L8S 4L7
gadsdesa@mcmaster.ca

## ABSTRACT

*This article discusses the application of a novel model-based fault detection method. The method is based on the interacting multiple model (IMM) strategy, which makes use of a finite number of known operating modes. A filter is used in conjunction with the IMM in order to estimate the states and parameters of the system. The smooth variable structure filter (SVSF) is a relatively new estimation strategy, and is based on sliding mode concepts which introduces an inherent amount of robustness and stability. The combined SVSF-IMM strategy is applied on an electrohydrostatic actuator (EHA), which is a device used in the aerospace industry. Two different operating modes were created, based on varying degrees of friction acting on the EHA cylinder. The results of the friction fault detection were compared with the popular Kalman filter (KF) based IMM strategy.*

## NOMENCLATURE

$e$ Measurement (output) error vector or values
$j$ Number of filters (i.e., models used by the IMM)
$p$ Mode probability transition matrix
$u$ Input to the system
$v$ Measurement noise vector
$w$ System noise vector
$x$ State vector or values
$y$ Artificial measurement vector or values
$z$ Measurement (system output) vector or values
$A$ Linear system (process) transition matrix
$B$ Input gain matrix
$C$ Linear measurement (output) matrix
$G$ Transfer function (i.e., normal or friction)
$K$ Filter gain matrix (i.e., KF or SVSF)
$P$ State error covariance matrix
$Q$ System noise covariance matrix
$R$ Measurement noise covariance matrix
$S$ Innovation (measurement error) covariance matrix
$T$ Transpose of some vector or matrix
$\gamma$ SVSF ‘convergence’ or memory parameter
$\Lambda$ Likelihood term
$\mu$ Mode probability vector
$\psi$ SVSF smoothing boundary layer width
$|a|$ Absolute value of some parameter $a$
^ Estimated vector or values

Note that the subscripts $k+1|k$ and $k+1|k+1$ refer to a priori (i.e., before the fact) and a posteriori (i.e., after the fact) values of some parameter.

## INTRODUCTION

Fault detection and diagnosis methodologies are important for the successful control of mechanical and electrical systems. In the presence of a fault, the system behaviour may become unpredictable, resulting in a loss of control which can cause unwanted downtime as well as damage to the system. A variety of fault detection strategies have been introduced overtime in literature, and are typically considered as signal-based or model-based [1]. Signal-based fault detection methods typically use thresholds to extract information from available measurements [2,3]. This information is then used to determine if a fault is present. Model-based methods, as the name suggests, utilize faults that can be modeled, typically through system identification. This type of fault detection and diagnosis is popular when well-defined models can be created and used by model-based strategies.

The earliest developments of fault detection methodologies began in the 1970s, where observer-based fault detection strategies were proposed for linear systems [4,5,6]. In 1978, a first book appeared on model-based methods for fault detection and diagnosis, with applications on chemical processes [4,7]. A summary of early developments in fault-detection methods based on modeling and state estimation may be found in [8]. Multiple model (MM) approaches were originally presented in [9]. These approaches assumed that the system may be modeled or behaves according to one of a finite number of modes [10]. Static MM estimators were developed, which assumed that the system model does not change over time, and no switching occurs between models during the estimation process [10]. The overall estimator is considered dynamic, even though the individual models stay fixed. Dynamic MM estimators undergo switching over time. Based on a mode transition probability, it is possible that soft switching occurs, such that the mode switches (or jumps) to another model or process [10]. The actual interacting multiple model (IMM) algorithm was derived and presented in the 1980s [11,12]. The use of IMM for failure detection was first demonstrated in 1998 [13]. It is well established in literature that this strategy is more effective than the static MM estimator [10].

Essentially, the IMM makes use of a number of models (i.e., for each fault condition), and is associated with filters that run in parallel. The output from each filter includes the state estimate, the covariance, and the likelihood calculation (which is a function of the measurement error and innovation covariance). The output from the filters is used to calculate fault probabilities, which gives an indication of how close the filtered model is to the true fault model. The IMM has been shown to work significantly better than single model methods, since it is able to make use of more information [10]. It also works extremely well for standard estimation problems such as target tracking, where there are typically two models used (i.e., the planes behaves according to uniform motion or coordinated turn models) [10].

The standard IMM employs the use of the Kalman filter (KF), which is a very popular and well-studied estimation method. Introduced in the early 1960's, it yields a statistically optimal solution for linear estimation problems in the presence of Gaussian noise [14]. In other words, based on the available information on the system, it yields the best possible solution in terms of estimation error [15]. The KF is formulated in a predictor-corrector manner, such that one first predicts the state estimates using knowledge of the system model. These estimates are termed as a priori, meaning 'prior to' knowledge of the observations. A correction term is then added based on the innovation (also called residuals or measurement errors), thus forming the updated or a posteriori (meaning 'subsequent to' the observations) state estimates [16].

The KF assumes that the system model is known and is linear, the system and measurement noises are white, and the states have initial conditions and are modeled as random variables with known means and variances [10,17]. However, these assumptions do not always hold in real applications. If one of these assumptions is violated, the KF performance becomes sub-optimal and could potentially become unstable [18]. Moreover, the KF is sensitive to the machines arithmetic precision and the complexity of the calculation (in particular, the inversion operator). The smooth variable structure filter (SVSF) was introduced in an effort to provide a more stable filter, while maintaining a relatively good estimate [19,20]. The SVSF is a type of sliding mode estimator, where gain switching is used to ensure that the estimates converge to within a boundary of the true state values (i.e., existence subspace) [21]. In its present form, the SVSF is stable and robust to modeling uncertainties and noise, given an upper bound on the level of un-modeled dynamics or knowledge of the magnitude of noise. It has been shown to work very well when the system is not well-defined or there are modeling errors.

In this paper, the SVSF is combined with the IMM strategy in an effort to detect friction faults on an experimental apparatus. The results of the experiment are compared with the popular KF-IMM. The paper is organized as follows. The SVSF estimation method is presented next, followed by the SVSF-IMM strategy. The experimental setup is described, followed by the results. The paper concludes with a summary of the main findings.

## SMOOTH VARIABLE STRUCTURE FILTER

A new form of predictor-corrector estimator based on sliding mode concepts referred to as the variable structure filter (VSF) was introduced in 2003 [19]. Essentially this method makes use of the variable structure theory and sliding mode concepts. It uses a switching gain to converge the estimates to within a boundary of the true state values (i.e., existence subspace). In 2007, the smooth variable structure filter (SVSF) was derived which makes use of a simpler and less complex gain calculation [20]. In its present form, the SVSF has been shown to be stable and robust to modeling uncertainties and noise, when given an upper bound on the level of un-modeled dynamics and noise [19,22]. The basic estimation concept of the SVSF is shown in Fig. 1.

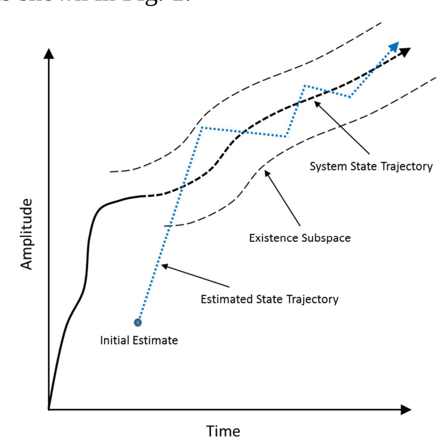


FIGURE 1. SVSF ESTIMATION CONCEPT

The SVSF method is model based and may be applied to differentiable linear or nonlinear dynamic equations. The original form of the SVSF as presented in [20] did not include covariance derivations. An augmented form of the SVSF was presented in [23], which includes a full derivation for the filter. The estimation process is iterative and may be summarized by the following set of equations (for linear systems). The predicted state estimates $\hat{x}_{k+1|k}$ and state error covariances $P_{k+1|k}$ are first calculated respectively as follows:

$$\hat{x}_{k+1|k} = A\hat{x}_{k|k} + Bu_k \tag{1}$$

$$P_{k+1|k} = AP_{k|k}A^T + Q_{k+1} \tag{2}$$

Utilizing the predicted state estimates $\hat{x}_{k+1|k}$, the corresponding predicted measurements $\hat{z}_{k+1|k}$ and measurement errors $e_{z,k+1|k}$ may be calculated:

$$\hat{z}_{k+1|k} = C\hat{x}_{k+1|k} \tag{3}$$

$$e_{z,k+1|k} = z_{k+1} - \hat{z}_{k+1|k} \tag{4}$$

The SVSF process differs from the KF in how the gain is formulated. The SVSF gain is a function of: the a priori and the a posteriori measurement errors $e_{z,k+1|k}$ and $e_{z,k|k}$; the smoothing boundary layer widths $\psi$; the 'SVSF' memory or convergence rate $\gamma$; as well as the measurement matrix $C$. For the derivation of the gain $K_{k+1}$, refer to [20,23]. The SVSF gain is defined as a diagonal matrix such that:

$$\begin{aligned}K_{k+1} = C^{-1} diag\Big[\Big(\left|e_{z_{k+1|k}}\right| + \gamma\left|e_{z_{k|k}}\right|\Big)\\ \circ\, sat\left(\psi^{-1}e_{z_{k+1|k}}\right)\Big]\, diag\left(e_{z_{k+1|k}}\right)^{-1}\end{aligned} \tag{5}$$

Where $\circ$ signifies Schur (or element-by-element) multiplication, and where $\psi^{-1}$ is a diagonal matrix constructed from the constant smoothing boundary layer widths, such that:

$$\psi^{-1} = \begin{bmatrix} \frac{1}{\psi_1} & 0 & 0 \\ 0 & \ddots & 0 \\ 0 & 0 & \frac{1}{\psi_m} \end{bmatrix} \tag{6}$$

Note that $m$ is the number of measurements, and the saturation function of (5) is defined by:

$$sat\left(\psi^{-1}e_{z_{k+1|k}}\right) = \begin{cases} 1, & e_{z_i,k+1|k}/\psi_i \geq 1 \\ e_{z_i,k+1|k}/\psi_i, & -1 < e_{z_i,k+1|k}/\psi_i < 1 \\ -1, & e_{z_i,k+1|k}/\psi_i \leq -1 \end{cases} \tag{7}$$

This gain is used to calculate the updated state estimates $\hat{x}_{k+1|k+1}$ as well as the updated state error covariance matrix $P_{k+1|k+1}$:

$$\hat{x}_{k+1|k+1} = \hat{x}_{k+1|k} + K_{k+1}e_{z,k+1|k} \tag{8}$$

$$\begin{aligned}P_{k+1|k+1} = (I - K_{k+1}C)P_{k+1|k}(I - K_{k+1}C)^T\\ + K_{k+1}R_{k+1}K_{k+1}^T\end{aligned} \tag{9}$$

Finally, the updated measurement estimate $\hat{z}_{k+1|k+1}$ and measurement errors $e_{z,k+1|k+1}$ are calculated, and are used in later iterations:

$$\hat{z}_{k+1|k+1} = C\hat{x}_{k+1|k+1} \tag{10}$$

$$e_{z,k+1|k+1} = z_{k+1} - \hat{z}_{k+1|k+1} \tag{11}$$

The existence subspace shown in Figs. 1 and 2 represents the amount of uncertainties present in the estimation process, in terms of modeling errors or the presence of noise. The width of the existence space $\beta$ is a function of the uncertain dynamics associated with the inaccuracy of the internal model of the filter as well as the measurement model, and varies with time [20]. Typically this value is not exactly known but an upper bound may be selected based on a priori knowledge. Once within the existence boundary subspace, the estimated states are forced (by the SVSF gain) to switch back and forth along the true state trajectory. High-frequency switching caused by the SVSF gain is referred to as chattering, and in most cases, is undesirable for obtaining accurate estimates [20]. However, the effects of chattering may be minimized by the introduction of a smoothing boundary layer $\psi$. The selection of the smoothing boundary layer width reflects the level of uncertainties in the filter and the disturbances (i.e., system and measurement noise, and un-modeled dynamics).

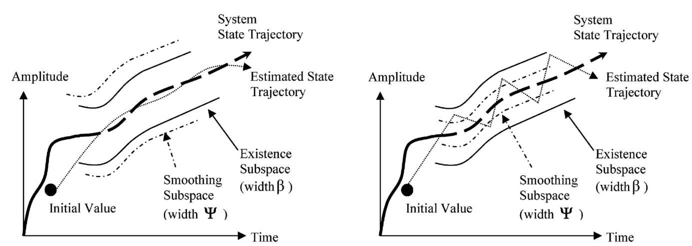


(A) SMOOTHING ($\psi \geq \beta$) (B) CHATTERING ($\psi < \beta$)

FIGURE 2. SMOOTHING BOUNDARY LAYER [20]

The effect of the smoothing boundary layer is shown in Fig. 2. When the smoothing boundary layer is defined larger than the existence subspace boundary, the estimated state trajectory is smoothed. However, when the smoothing term is too small, chattering remains due to the uncertainties being underestimated. The SVSF proof of stability is well established and is available in [20] and [24].

The SVSF provides an estimation process that is sub-optimal albeit robust and stable. It is hence beneficial to be able to combine the accurate performances of the KF with the stability of the SVSF. A recent development, as described in [25], provides a methodology for calculating a variable smoothing boundary layer $\psi$. The partial derivative of the a posteriori covariance (trace) with respect to the smoothing boundary layer term $\psi$ is the basis for obtaining an optimal, time-varying strategy for the specification of $\psi$. In linear systems, this smoothing boundary layer yields an optimal gain, similar to the KF.

Previous forms of the SVSF included a vector form of $\psi$, which had a single smoothing boundary layer term for each corresponding measurement error [20]. Essentially, the boundary layer terms were independent of each other such that the measurement errors would not mix when calculating the corresponding gain, leading to a loss of optimality. A 'near-optimal' formulation of the SVSF could be created using a vector form of $\psi$, however this would lead to a minimization of only the diagonal elements of the state error covariance matrix [26]. In an effort to obtain a smoothing boundary layer equation that yielded optimal state estimates, a full smoothing boundary layer matrix was proposed in [25]. Hence, consider the full matrix form of the smoothing boundary layer:

$$\psi = \begin{bmatrix} \psi_{11} & \psi_{12} & \cdots & \psi_{1m} \\ \psi_{12} & \psi_{22} & \cdots & \psi_{2m} \\ \vdots & \vdots & \ddots & \vdots \\ \psi_{m1} & \psi_{m2} & \cdots & \psi_{mm} \end{bmatrix} \tag{12}$$

This definition includes terms that relate one smoothing boundary layer to another (i.e., off-diagonal terms). To solve for the optimal smoothing boundary layer based on (12), consider:

$$\frac{\partial\left(trace[P_{k+1|k+1}]\right)}{\partial\psi} = 0 \tag{13}$$

As described in [25], a solution for the smoothing boundary layer from (13) is defined as follows:

$$\psi_{k+1} = \left(\bar{E}^{-1} C P_{k+1|k} C^T S_{k+1}^{-1}\right)^{-1} \tag{14}$$

Where $E$ is defined as follows:

$$E = \left(\left|e_{z_{k+1|k}}\right| + \gamma\left|e_{z_{k|k}}\right|\right) \tag{15}$$

Note that in (14), $\bar{E}$ refers to forming a diagonal matrix of elements consisting of $E$. The KF and SVSF strategies may be combined using this smoothing boundary layer calculation, which leads to an accurate and robust estimation strategy [25]. Furthermore, the smoothing boundary layer width (14) also provides another indicator for determining the presence of faults, as will be demonstrated experimentally later. Consider the following sets of figures to help describe the overall implementation of the SVSF strategy used in this paper and proposed in [25].

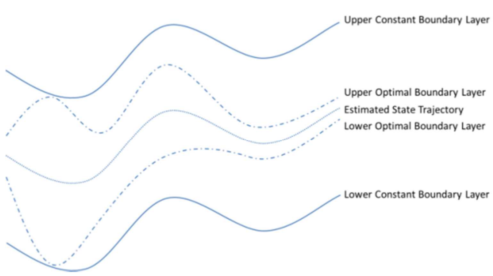


FIGURE 3. BOUNDARY LAYER CONCEPT FOR WELL-DEFINED CASE [25]

Figure 3 illustrates the case when the constant smoothing boundary layer width used by the SVSF is defined larger than the optimal smoothing boundary layer (i.e., a conservative choice) calculated by (14). The difference between the constant and upper layers leads to a loss in optimality for the SVSF. Essentially, in this case, the KF gain should be used to obtain the best result.

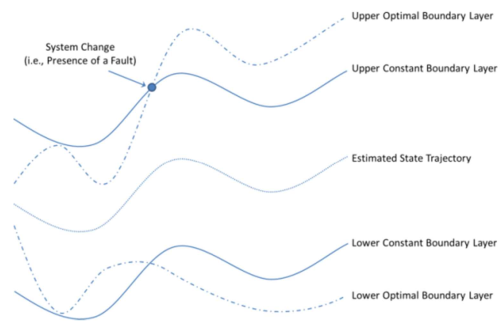


FIGURE 4. PRESENCE OF FAULT OR POORLY-DEFINED SYSTEM CASE [25]

Figure 4 illustrates the case when the optimal smoothing boundary layer is calculated to exist beyond the constant smoothing boundary layer. This typically occurs when there is modeling uncertainty (which leads to a loss in optimality) that exceed the limits of a constant smoothing boundary layer. The limits are set by the width of the existence subspace, which was discussed earlier. In a situation defined by Fig. 4 when $\psi_{opt} \geq \psi_{con}$, to ensure a stable estimate, the SVSF gain (5) should be used to update the state estimates. The smoothing boundary layer widths calculated by (14) are saturated at the constant values. This ensures a stable estimate, as defined by the proof of stability for the SVSF [20,24]. Furthermore, to improve the SVSF results (i.e., without the use of (14)), the averaged smoothing boundary layers (for the well-defined system) can be used to set the constant boundary layer widths. Doing so provides a well-tuned existence subspace that yields more accurate estimates.

## OVERVIEW OF THE SVSF-IMM STRATEGY

The standard IMM strategy was implemented as per Section 11.6 of [10]. The overall concept is shown in Fig. 5. Essentially, any estimation strategy (with a covariance derivation) may be applied on the models of interest. In this case, there are two models. Prior to feeding the initial estimates and covariance's into the filter models, an interaction (mixing) stage takes place, as per the following equations. The predicted mode probability μ, as defined by (16), is first calculated based on the mode transition matrix $p$ (user defined) and the previous (or initial) mode probabilities.

$$\mu_{i|j_{k|k}} = \frac{1}{\bar{c}^j} p_{ij}\mu_{i_k} \tag{16}$$

$$\bar{c}_j = \sum_{i=1}^{r} p_{ij}\mu_{i_k} \tag{17}$$

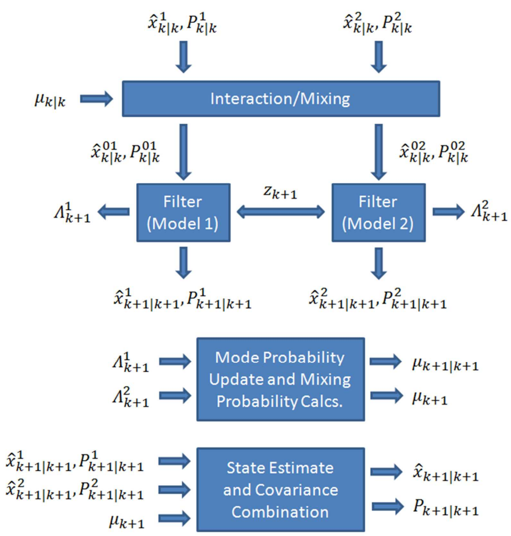


FIGURE 5. IMM STRATEGY (ADAPTED FROM [10])

The mode probabilities are used like weights to determine the corresponding initial estimates (18) and covariance (19).

$$\hat{x}^{0j}_{k|k} = \sum_{i=1}^{r} \hat{x}^{i}_{k|k} \mu_{i|j_{k|k}} \tag{18}$$

$$P^{0j}_{k|k} = \sum_{i=1}^{r} \mu_{i|j_{k|k}} \left\{ P^{i}_{k|k} + \left[\hat{x}^{i}_{k|k} - \hat{x}^{0j}_{k|k}\right]\left[\hat{x}^{i}_{k|k} - \hat{x}^{0j}_{k|k}\right]^T \right\} \tag{19}$$

Using these values and the measurement as inputs, the SVSF calculates the corresponding state estimates and covariance (for each model), as described by (1) – (15). Based on the a priori measurement error (4) and the innovation matrix (20), a likelihood function $\Lambda$ may be calculated for each model $j$, as follows:

$$S_{k+1|k} = C P_{k+1|k} C^T + R_{k+1} \tag{20}$$

$$\Lambda^{j}_{k+1} = \frac{1}{\sqrt{\left|2\pi S^{j}_{k+1|k}\right|}} exp\left( \frac{-0.5\left(e^{j}_{z_{k+1|k}}\right)^T e^{j}_{z_{k+1|k}}}{S^{j}_{k+1|k}} \right) \tag{21}$$

These likelihood functions $\Lambda$ are used to determine updates to the mode probability (22) and mixing calculations, as follows:

$$\mu_{j_{k+1}} = \frac{1}{c_j} \Lambda^{j}_{k+1} \bar{c}_j \tag{22}$$

$$c_j = \sum_{j=1}^{r} \Lambda^{j}_{k+1} \bar{c}_j \tag{23}$$

Furthermore, the two sets of state estimates and covariance's may be combined (for output purposes only) to determine the IMM estimate of the respective filter (i.e., KF or SVSF), as per (24) and (25) [10]:

$$\hat{x}_{k+1|k+1} = \sum_{j=1}^{r} \hat{x}^{j}_{k+1|k+1} \mu_{j_{k+1}} \tag{24}$$

$$P_{k+1|k+1} = \sum_{j=1}^{r} \mu^{j}_{k+1} \left\{ P^{j}_{k+1|k+1} + \left[\hat{x}^{j}_{k+1|k+1} - \hat{x}_{k+1|k+1}\right] \cdot \right. \\ \left. \cdot \left[\hat{x}^{j}_{k+1|k+1} - \hat{x}_{k+1|k+1}\right]^T \right\} \tag{25}$$

The main SVSF-IMM process and equations are defined by (16) through (25), where there are $\mathrm{i}, \mathrm{j} = 1, \dots, \mathrm{r}$ models.

## EXPERIMENTAL SETUP

The experimental setup used in this paper involved an electrohydrostatic actuator (EHA). An EHA is an emerging type of actuator typically used in the aerospace industry, and are self-contained units comprised of their own pump, hydraulic circuit, and actuating cylinder [22]. The main components of an EHA include a variable speed motor, an external gear pump, an accumulator, inner circuitry check valves, a double-rod double-acting cylinder, and a bi-directional pressure relief mechanism. The experimental setup used in this paper is shown in the following figure.

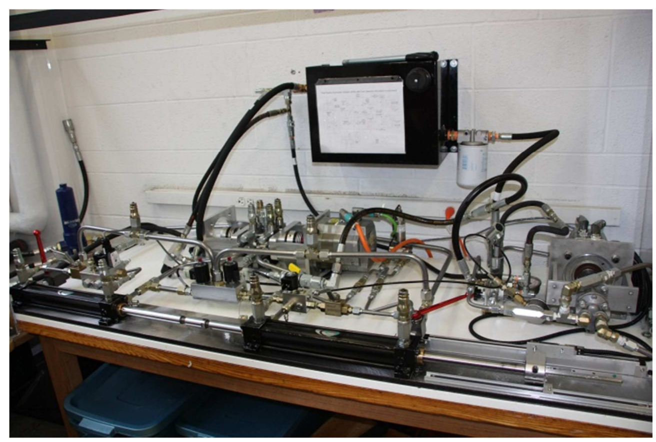

FIGURE 6. EHA EXPERIMENTAL SETUP

The EHA can be divided into two subsystems. The first is the inner circuit that includes the accumulator and its surrounding check valves. The second is the high pressure outer circuit which performs the actuation. The inner circuit prevents cavitation which occurs when the inlet pressure reaches near vacuum pressures and provides make-up fluid for any dynamic leakage [22]. This section is statically charged to $276\, kPa$ ($40\, psi$) which is enough pressure to avoid cavitation but it is also low enough to allow flow from the case drain back into the circuit. The inner circuit during normal operation is negligible in mathematical modeling. Mathematical modeling of the EHA has been performed and can be seen in detail in [22].

A dual version of the EHA was developed that places two systems in series by rigidly attaching the shafts of both cylinders to one another [27]. This system also includes two 2-way, normally closed solenoid valves that act as bypass valves in the event of a fault. This allows one pump to drive both cylinders if needed. There are also valves used to connect the inlet and outlet lines of both axes to each other. This provides a steady motion if the actuation of both pumps are not equal. The inclusion of the throttling valves also allows for fault simulations.

A friction fault is introduced to this system, and is used to demonstrate the performance of the SVSF-IMM. To incur this fault, one of the axes will be used as the driving mechanism while the other will act as a load. A pump is used to drive both cylinders, while the second axis blocking valve is in the closed position for all of the scenarios. In this case, the valve that allows fluid to flow between both chambers of the second cylinder is its corresponding throttle valve. This valve, along with its counterpart on the first cylinder, is a normally open, 2-way, bi-directional proportional valve that receives an $0-10\,V$ input from the controller. The increased throttling of this valve while the cylinder is in motion increases the back pressure, which simulates increased friction in the system.

System identification was performed in an effort to extract a 'black box model' of a dynamic system by fitting a statistical model with experimental measurements and designer knowledge of the system. The prior knowledge of the system includes the frequency range of interest, saturation, and knowledge of the piece-wise linear regions. To create an accurate model, the frequency of interest should include the frequency range up to the break-frequency, after which the signal-to-noise ratio drops dramatically and stops offering valuable information. However, the friction affects the system performance mainly at low frequencies, such that the input frequency of the test was limited to $10\,Hz$. The saturation of the system was tested with a ramp input by changing the throttling level of the second throttle valve. The velocity at which the system starts to saturate gradually decreases as the throttle valve input is increased. A dead band of the system was observed ($0.005\,m/s$), and is hypothesized to be a result of static friction present in the system. As a result, the operating amplitude was set to $2\,V$, which drives the system to avoid saturation and the dead band. In order to observe the friction effect on the system performance, a chirp signal with amplitude $2\,V$ and maximum frequency $10\,Hz$ was sent as an input. The friction effect was observed by looking at the magnitude change at low frequencies, and was found to be small compared with the magnitude of the measurement noise. Therefore, only two friction models were extracted (i.e., normal and high-friction). Future work will involve the use of an accelerometer (as opposed to a potentiometer) to obtain the velocity measurement of the axis position, in an effort to minimize the effects of noise, such that more distinct friction models may be obtained and studied. Measurements were obtained by inputting $30\,Hz$ pseudo-random binary signals (PRBS) with amplitude $2\,V$, filtered with a $10\,Hz$ low-pass filter. The system output was filtered with a zero-phase low-pass filter, with a band pass of $10\,Hz$. Two system transfer functions were created by fitting Box-Jenkins models with experimental data, and are defined (in discrete-time, with $T = 0.001\,s$) as follows:

$$G_{Normal} = \frac{5.0\times10^{-3}z^2 - 9.5\times10^{-3}z + 4.6\times10^{-3}}{z^3 - 1.952z^2 + 0.952z} \tag{26}$$

$$G_{Friction} = \frac{4.7\times10^{-3}z^2 - 9.0\times10^{-3}z + 4.4\times10^{-3}}{z^3 - 1.963z^2 + 0.963z} \tag{27}$$

Equation (26) describes the normal transfer function model, and (27) refers to the model when friction is present in the system. These transfer functions were transformed into their respective state-space representation (i.e., observable canonical form) [28]. For the normal model, the system and gain matrices were found respectively as:

$$A_{Normal} = \begin{bmatrix} 1.952 & 1 & 0 \\ -0.952 & 0 & 1 \\ 0 & 0 & 0 \end{bmatrix} \tag{28}$$

$$B_{Normal} = [5.0\times10^{-3} \quad -9.5\times10^{-3} \quad 4.6\times10^{-3}]^T \tag{29}$$

Similarly, the system and gain matrices for the friction model were found as follows:

$$A_{Friction} = \begin{bmatrix} 1.963 & 1 & 0 \\ -0.963 & 0 & 1 \\ 0 & 0 & 0 \end{bmatrix} \tag{30}$$

$$B_{Friction} = [4.7\times10^{-3} \quad -9.0\times10^{-3} \quad 4.4\times10^{-3}]^T \tag{31}$$

The measurement matrix is the same for both cases, and is defined as:

$$C = [1 \quad 0 \quad 0] \tag{32}$$

Note that the states for this system are of kinematic type: velocity $(\mathrm{m/s})$, acceleration $(\mathrm{m/s^2})$, and jerk $(\mathrm{m/s^3})$. It is not uncommon to have fewer measurements than states. However, the SVSF gain defined by (5) requires a square measurement matrix. In this case, different strategies may be used to extract the appropriate information and create 'artificial' measurements y. A number of methods exist, such as the reduced order or Luenberger's approach, which are presented in [20,29,30]. For example, in the case of phase variables, it is possible to derive acceleration from velocity, such that:

$$y_{2,k} = \frac{1}{T}\left(z_{1,k+1} - z_{1,k}\right) \tag{33}$$

Likewise, the third artificial measurement may be extracted:

$$y_{3,k} = \frac{1}{T}\left(z_{2,k+1} - z_{2,k}\right) \tag{34}$$

The accuracy of (33) and (34) depends on the sampling rate T. Applying (34) and (34) allows a measurement matrix equivalent to the identity matrix. The estimation process would continue as in the previous section, where a full measurement matrix was available. Note however that the artificial measurements would be delayed a time step. If the system models (28) – (31) are known with complete confidence, then it is possible to derive an artificial measurement for the acceleration from the first measurement based on the models. This method has been explored and reported in [25].

## EXPERIMENTAL RESULTS

To obtain the experimental results, note that the constant smoothing boundary layer width was set to $\psi_i = 5 \times 10^3$ for each boundary ($i = 1,2,3$), and the SVSF 'memory' was defined as $\gamma = 0.1$. An exact value of the system noise covariance matrix $Q$ was not available from the experimental setup. Although some adaptive methods exist for obtaining estimates of a noise covariance, the values used in this paper were obtained by trial-and-error. It was found that a very small value for the system noise covariance yielded good results for both filters, such that $Q = 10^{-9} \times diag([1 \quad 1 \quad 1])$. To obtain an estimate of the measurement noise covariance matrix $R$, a portion of the measurement signal was extracted and analyzed. For this experiment, it was determined that $R = 6.36 \times 10^{-7}$.

The input to the system (through velocity control of the motor) consisted of a series of step inputs: $+2V$ for the first 2.5 seconds, followed by $-2V$ for another 2.5 seconds, and $+2V$ for the remainder of time. For the first step, the normal model was applied. At the start of the second step, the friction fault was present. The last step involved normal operation. The measurements obtained from the sensor yielded (after applying a zero-phase filter) the following velocity profile.

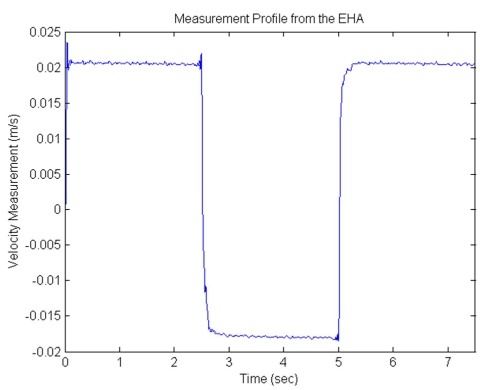


FIGURE 7. MEASUREMENT PROFILE FROM THE EHA

Both the popular KF-IMM and new SVSF-IMM strategies were applied on the experimental setup in an effort to determine the presence of faults. The next two figures illustrate the mode probabilities for both the normal and friction models. A value of 1 indicates that the model is currently being used by the system, whereas a value of 0 indicates that the model is not present in the system dynamics. For example, the true mode probability value for the normal model should be 1 for the first 2.5 seconds, followed by 0 for 2.5 seconds, and then 1 for the remainder. As demonstrated by Fig.'s 8 and 9, both strategies are able to successfully detect and diagnosis the presence of the friction fault when it is implemented in the system at 2.5 seconds. However, note that the SVSF-IMM strategy is able to calculate the correct mode probability by a higher percentage. For example, when the system is operating normally, the SVSF-IMM strategy correctly identifies the normal mode by about 20% more than the KF-IMM strategy.

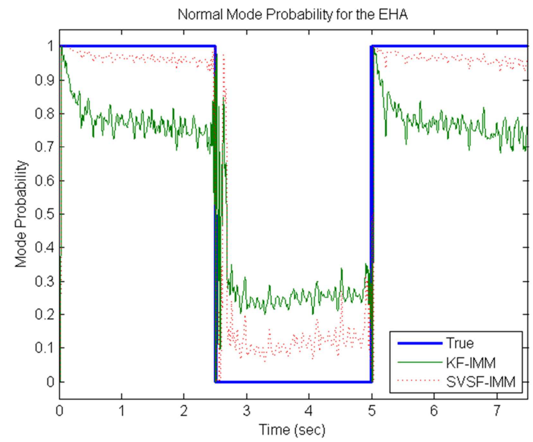


FIGURE 8. NORMAL MODE PROBABILITY RESULTS

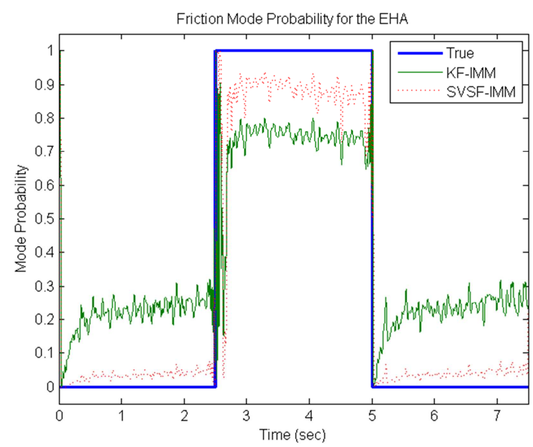


FIGURE 9. FRICTION MODE PROBABILITY RESULTS

The results of the estimation process may be summarized by the following table. Both strategies were able to provide a very good estimate of the three system states. The root mean squared error (RMSE) was calculated and is listed in Tab. 1. However, note that the true system values were not available for the EHA. Therefore, designer knowledge was used to create artificial 'noiseless' states based on the models (26) and (27), and when the friction fault was introduced. These 'true' state values were used to calculate the RMSE of the estimates. For this case, it was found that the SVSF-IMM provided roughly twice as accurate results when compared with the KF-IMM strategy, in terms of estimation error.

TABLE 1. ESTIMATED RMSE RESULTS

| **Strategy** | **Velocity** $(m/s)$ | **Acceleration** $(m/s^2)$ | **Jerk** $(m/s^3)$ |
|---|---|---|---|
| KF-IMM | $7.53 \times 10^{-4}$ | $7.71 \times 10^{-4}$ | $1.12 \times 10^{-4}$ |
| SVSF-IMM | $3.38 \times 10^{-4}$ | $3.67 \times 10^{-4}$ | $5.91 \times 10^{-5}$ |

As previously mentioned, the time-varying (or optimal solution to the) smoothing boundary layer defined by (14) also yields another indicator of when a fault (or system change) occurs. Consider the following figure which illustrates the smoothing boundary layer for the velocity state, over time. The spikes present at 2.5 and 5 seconds indicate that the system experienced a change in its dynamics. This can be confirmed by the mode probability calculations (Fig.'s 8 and 9).

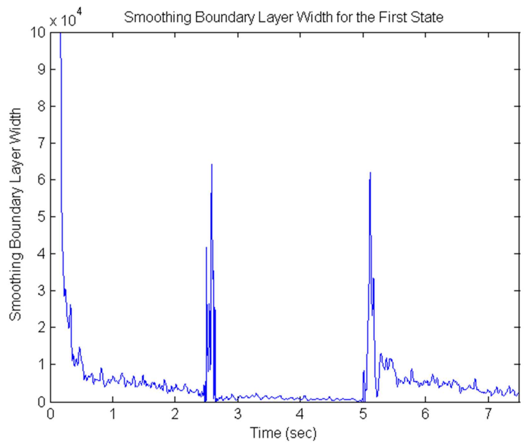


FIGURE 10. INDICATION OF A SYSTEM CHANGE

## CONCLUSIONS

This article discussed the application of a novel model-based fault detection method. The relatively new SVSF estimation strategy was combined with the IMM method. The fault detection strategy was applied on an experimental setup, and the results were compared with the popular KF-IMM. It was determined that the SVSF-IMM method yielded a higher fault detection probability, and more accurate estimates. Future work will study the sensitivity of the strategy to minor faults.

## ACKNOWLEDGMENTS

The authors would like to thank Mohammed El Sayed (McMaster University) for his support and helpful discussions.

## REFERENCES

[1] R. Isermann, "Model-Based Fault Detection and Diagnosis - Status and Applications," *Annual Reviews in Control*, vol. 29, no. 1, pp. 71-85, 2005.

[2] Y. Wang, Y. Xing, and H. He, "An Intelligent Approach for Engine Fault Diagnosis Based on Wavelet Pre-Processing Neural Network Model," in *IEEE International Conference on Information and Automation*, 2010, pp. 576-581.

[3] J. Korbicz, "Artificial Neural Networks in Fault Diagnosis of Dynamical Systems," in *IEEE Region 8 International Conference on Computational Technologies in Electrical and Electronics Engineering*, 2010, p. 449.

[4] R. Isermann and P. Balle, "Trends in the Application of Model-Based Fault Detection and Diagnosis of Technical Processes," *Control Engineering Practice*, vol. 5, no. 5, pp. 709-719, May 1997.

[5] R. V. Beard, "Failure Accomodation in Linear systems Through Self-Reorganization," Man Vehicle Lab, Cambridge, Massachusetts, MVT-71-1, 1971.

[6] H. L. Jones, "Failure Detection in Linear Systems," Department of Aeronautics, M.I.T., Cambridge, Massachusetts, Ph.D. Thesis 1973.

[7] D. M. Himmelblau, *Fault Detection and Diagnosis in Chemical and Petrochemical Processes*. Amsterdam: Elsevier, 1978.

[8] R. Isermann, "Process Fault Detection Based on Modelling and Estimation Methods: A Survey," *Automatica*, vol. 20, 1984.

[9] D. T. Magill, "Optimal Adaptive Estimation of Sampled Stochastic Processes," *IEEE Transactions on Automatic Control*, vol. 10, pp. 434-439, 1965.

[10] Y. Bar-Shalom, X. Rong Li, and T. Kirubarajan, *Estimation with Applications to Tracking and Navigation*. New York: John Wiley and Sons, Inc., 2001.

[11] H. A. P. Blom, "An Efficient Filter for Abruptly Changing Systems," in *Proceedings of the 23rd IEEE Conference on Decision and Control*, Las Vegas, Nevada, December, 1984.

[12] H. A. P. Blom and Y. Bar-Shalom, "The Interacting Multiple Model Algorithm for Systems with Markovian Switching Coefficients," *IEEE Transactions on Automatic Control*, vol. 33, no. 8, pp. 780-783, August 1988.

[13] Y. M. Zhang and X. R. Li, "Detection and Diagnosis of Sensor and Actuator Failures Using IMM Estimator," *IEEE Transactions on Aerospace and Electronic Systems*, pp. 1293-1313, October 1998.

[14] R. E. Kalman, "A New Approach to Linear Filtering and Prediction Problems," *Journal of Basic Engineering, Transactions of ASME*, vol. 82, pp. 35-45, 1960.

[15] B. D. O. Anderson and J. B. Moore, *Optimal Filtering*. Englewood Cliffs, NJ: Prentice-Hall, 1979.

[16] G. Welch and G. Bishop, "An Introduction to the Kalman Filter," Department of Computer Science, University of North Carolina, 2006.

[17] D. Simon, *Optimal State Estimation: Kalman, H-Infinity, and Nonlinear Approaches*.: Wiley-Interscience, 2006.

[18] A. Gelb, *Applied Optimal Estimation*. Cambridge, MA: MIT Press, 1974.

[19] S. R. Habibi and R. Burton, "The Variable Structure Filter," *Journal of Dynamic Systems, Measurement, and Control (ASME)*, vol. 125, pp. 287-293, September 2003.

[20] S. R. Habibi, "The Smooth Variable Structure Filter," *Proceedings of the IEEE*, vol. 95, no. 5, pp. 1026-1059, 2007.

[21] V. I. Utkin, *Sliding Mode and Their Application in Variable Structure Systems*, English Translation ed.: Mir Publication, 1978.

[22] S. R. Habibi and R. Burton, "Parameter Identification for a High Performance Hydrostatic Actuation System using the Variable Structure Filter Concept," *ASME Journal of Dynamic Systems, Measurement, and Control*, 2007.

[23] S. A. Gadsden and S. R. Habibi, "A New Form of the Smooth Variable Structure Filter with a Covariance Derivation," in *IEEE Conference on Decision and Control*, Atlanta, Georgia, 2010.

[24] M. Al-Shabi, "The General Toeplitz/Observability SVSF," Department of Mechanical Engineering, McMaster University, Hamilton, Ontario, Ph.D. Thesis 2011.

[25] S. A. Gadsden and S. R. Habibi, "An Optimal Smoothing Boundary Layer for the Smoth Variable Structure Filter," *Journal of Dynamic Systems, Measurements and Control (ASME)*, Submitted February 2, 2011 (DS-11-1025).

[26] S. A. Gadsden, M. El Sayed, and S. R. Habibi, "Derivation of an Optimal Boundary Layer Width for the Smooth Variable Structure Filter," in *American Control Conference*, San Francisco, CA, USA, 2011.

[27] K. R. McCullough, "Design and Characterization of a Dual Electro-Hydrostatic Actuator," Department of Mechanical Engineering, McMaster University, Hamilton, Ontario, M.A.Sc. Thesis 2011.

[28] K. Ogata, *Discrete-Time Control Systems*, 2nd ed. U.S.A.: Prentice Hall, 1994.

[29] T. Kailath, *Linear Systems*. U.S.A.: Prentice Hall, 1980.

[30] D. G. Luenberger, *Introduction to Dynamic Systems*. U.S.A.: John Wiley, 1979.